JGR Planets

RESEARCH ARTICLE
10.1029/2021JE007168

Key Points:

- Using a dust accelerator, we shot polypyrrole-coated olivine particles at 10–20 km/s into a gas target containing air
- The particles differentially ablated their organic coatings in the form of large molecules
- The results suggest that meteors may deliver complex organics into planetary atmospheres and those organics may produce detectable charges

Correspondence to:
Z. Sternovsky,
zoltan.sternovsky@lasp.colorado.edu

Citation:
DeLuca, M., Sternovsky, Z., Armes, S. P., Fielding, L. A., Horányi, M., Janches, D., et al. (2022). Differential ablation of organic coatings from micrometeoroids simulated in the laboratory. *Journal of Geophysical Research: Planets*, *127*, e2021JE007168. https://doi.org/10.1029/2021JE007168

Received 19 DEC 2021
Accepted 30 MAR 2022

Author Contributions:
Conceptualization: Michael DeLuca, Zoltan Sternovsky
Data curation: Michael DeLuca
Formal analysis: Michael DeLuca, Zoltan Kupihar
Funding acquisition: Zoltan Sternovsky
Investigation: Michael DeLuca, Steven P. Armes, Lee A. Fielding, Mihály Horányi, Diego Janches, Zoltan Kupihar, Tobin Munsat, John M. C. Plane
Methodology: Michael DeLuca, Zoltan Sternovsky, Steven P. Armes, Tobin Munsat, John M. C. Plane
Project Administration: Zoltan Sternovsky
Resources: Zoltan Sternovsky, Steven P. Armes, Lee A. Fielding
Software: Michael DeLuca
Supervision: Zoltan Sternovsky, Mihály Horányi
Validation: Michael DeLuca, Lee A. Fielding, Diego Janches, Zoltan Kupihar, John M. C. Plane
Visualization: Michael DeLuca

Differential Ablation of Organic Coatings From Micrometeoroids Simulated in the Laboratory

Michael DeLuca[1,2,3], Zoltan Sternovsky[1,2], Steven P. Armes[4], Lee A. Fielding[5], Mihály Horányi[1,6], Diego Janches[7], Zoltan Kupihar[8], Tobin Munsat[6], and John M. C. Plane[9]

[1]Laboratory for Atmospheric and Space Physics, University of Colorado, Boulder, CO, USA, [2]Smead Department of Aerospace Engineering Sciences, University of Colorado, Boulder, CO, USA, [3]Now at Department of Astrophysical Sciences, Princeton University, Princeton, NJ, USA, [4]Department of Chemistry, University of Sheffield, Sheffield, UK, [5]Department of Materials, The University of Manchester, Manchester, UK, [6]Department of Physics, University of Colorado, Boulder, CO, USA, [7]NASA Goddard Space Flight Center, Greenbelt, MD, USA, [8]Department of Medicinal Chemistry, University of Szeged, Szeged, Hungary, [9]School of Chemistry, University of Leeds, Leeds, UK

Abstract Micrometeoroids contain organic material that may undergo differential ablation during atmospheric entry, potentially depositing organic material into Earth's atmosphere and affecting the radar detectability of meteors. To investigate the differential ablation of organics, we used a dust accelerator to shoot submicron polypyrrole-coated olivine particles at speeds of 10–20 km/s into a gas target containing air. A set of biased electrodes placed along the path of the particles measured the charges generated when the particles ablated and the ablated molecules collided with gas molecules. We observed that the particles differentially ablate their organic polypyrrole coatings prior to their inorganic olivine cores, producing spikes in charge production, with charge yields of 10^4–10^5 C/kg even at relatively low speeds. These measurements suggest that large organic molecules survived ablation and are responsible for the observed charge production since small molecules either do not produce ions at those speeds or produce them in much lower quantities than observed. We modeled the ablation using basic meteor physics by assuming that the polypyrrole coating decomposes into pyrrole monomer. Extending these results to the ablation of micrometeoroids in the atmosphere indicates that organic coatings should ablate at high altitudes within relatively narrow altitude ranges, which has consequences for the detectability of meteors by radar. Since the ablated coatings generate relatively large molecules, the results also suggest that micrometeoroids can deliver complex organic material into planetary atmospheres by ablating them during entry, potentially serving as a source of prebiotic organics.

Plain Language Summary Micrometeoroids entering the atmosphere heat up due to collisions with gas molecules and lose mass through ablation. The more volatile components ablate before the less volatile components, a process called differential ablation. To study how volatile organics in micrometeoroids will ablate, we shot olivine particles coated in polypyrrole, an organic conducting polymer, into a gas target at speeds of 10–20 km/s. The particles differentially ablated their polypyrrole coatings and produced charges when the ablated molecules collided with gas molecules. Using a set of electrically biased charge collectors located inside the target, we found that the coatings produced large amounts of charge, which suggest that large molecules survived ablation. This is because small molecules and atoms do not have the kinetic energy to produce ions when they collide with gas molecules. We modeled the process by assuming that the polypyrrole coating degrades to form pyrrole monomer. Our measurements suggest that organics ablated from micrometeoroids may produce sufficient charge to be detectable by radar. The apparent large size of the ablating molecules also suggests that meteors may be able to deliver complex organics into the atmosphere that could have been useful building blocks for life on the early Earth.

1. Introduction

As Earth orbits the Sun, it sweeps up fragments of comets and asteroids that ablate in its atmosphere. Most of these fragments are micrometeoroids with masses of 1 μg to 1 mg (Plane, 2012). As they ablate, these particles produce observable light and plasma while delivering exogenous material from comets and asteroids directly into the atmosphere. Meteoric ablation is a ubiquitous phenomenon that is not just relevant to Earth and is thus a critical field of research (Carillo-Sánchez et al., 2020; Janches et al., 2020).

Writing – original draft: Michael DeLuca
Writing – review & editing: Michael DeLuca, Zoltan Sternovsky, Steven P. Armes, Lee A. Fielding, Diego Janches, John M. C. Plane

In particular, the particles deliver organic material from asteroids and comets. Most of the mass influx to Earth are believed to be cometary in origin (Carrillo-Sánchez et al., 2016; Nesvorný et al., 2010, 2011). Comets are organic-rich, and dust particles originating from such sources can be up to 45% organics by mass (Bardyn et al., 2017). Some of these organic materials may then be delivered to Earth, provided it survives transfer through space and entry into the atmosphere. Typical micrometeorites and interplanetary dust particles collected on the ground or in the atmosphere can contain up to several percent organics by mass, and ultracarbonaceous Antarctic micrometeorites can be up to 85% organics by volume (Flynn et al., 2004; Koschny et al., 2019). Organic materials may also provide the "glue" that holds dust grains together. For instance, chondritic porous dust particles are aggregates of individual submicron grains with each grain coated in approximately 100 nm of organics (Flynn et al., 2013), and dustball models of meteors assume that micrometeoroids are bound together by a material with a low boiling point, which may be organic (e.g., Campbell-Brown & Koschny, 2004; Hawkes & Jones, 1975). These organics may be modified or destroyed during entry, depending on the level of heating (Anders, 1989; Riebe et al., 2020). A full understanding of meteors requires a more nuanced appreciation of how the organic fraction contributes to micrometeoroid ablation.

Where and how the organic material in micrometeoroids undergoes ablation may have implications for the radar detectability of meteors and the delivery of organic material to planets. In general, when a micrometeoroid containing volatile components enters the atmosphere, it undergoes differential ablation, in which the more volatile constituents of a micrometeoroid ablate first according to their vapourization temperatures (McNeil et al., 1998). Differential ablation has been observed by High Power and Large Aperture (HPLA) radars (Janches et al., 2009), and in the laboratory (Bones et al., 2016; Gómez Martín et al., 2017), and has been used to predict meteoric metal abundances in the atmosphere (e.g., Carillo-Sánchez et al., 2016; McNeil et al., 1998). However, these past studies focused on the differential ablation of metals and minerals, leaving open the question of how the volatile organic content behaves in this context.

If meteoric organics also ablate differentially, they could affect the radar detectability of meteors containing such material. The volatile elements (including Na and K) shed from meteoroids by differential ablation have large ionization efficiencies and are ablated over narrow altitude ranges. When elements and molecules ablate from meteoroids, they collide with atmospheric molecules and produce free electrons that are observable by radar. HPLA radars can observe the signatures produced by differential ablation. Differential ablation is essential to detecting slow micrometeoroids by sensitive radars since their heating is limited, and their nonvolatile constituents can remain mostly intact during atmospheric entry (Janches et al., 2014, 2015, 2017). Observations of differential ablation are important because detecting small and slow meteors is critical to constraining the mass flux to Earth and its sources. In particular, Nesvorný et al. (2010, 2011) suggested that the majority of Earth's mass influx is from slow and small particles from Jupiter Family Comets. However, detection of these particles by HPLA radars remains elusive (Janches et al., 2014, 2015, 2017). A better understanding of micrometeoroid ablation and detectability may help to resolve the discrepancy.

The ablation of meteoric organics is also relevant for determining the sources of Earth's organics prior to the origin of life. Earth formed in a region of the solar nebula that contained few volatiles owing to its relatively high temperature (Chyba & Hand, 2006), so any prebiotic organics present on the early Earth were either produced locally after Earth's formation or delivered from external sources. In particular, Anders (1989) and Chyba and Sagan (1992) suggested that interplanetary dust delivered significant quantities of organics to the early Earth. However, they focused on particles less than 1 μg in mass since more massive particles would be too strongly heated in the atmosphere for organics to survive. This limit excludes most of the meteoric mass inputs as potential providers of organics.

Despite the strong heating that micrometeoroids experience during entry, they could in principle still deliver organics by ablating them directly into the atmosphere (Jenniskens et al., 2000). If organics can survive the ablation, then meteors could be a significant source of organics because most of the incoming mass flux form meteors. There is some evidence for this scenario. Jenniskens et al. (2004) recorded spectra during the 2001 Leonid meteor storm and determined that organic molecules within the meteors were not broken apart by ablation. In addition, Glavin and Bada (2001) found that glycine, the simplest amino acid, survived sublimation from a piece of the Murchison meteorite when heated. There have also been observations of high-altitude ablation, which may be from organic materials (e.g., Elford et al., 1997; Murray et al., 1999; Rietmeijer, 2002; Spurný, Betlem, Jobse, et al., 2000; Spurný, Betlem, Leven, & Jenniskens, 2000). These studies suggest that meteor ablation

could provide a pathway for exogenous organic delivery, but determining its feasibility requires a more complete understanding of the ablation process.

Motivated by the relevance of organic ablation to meteor detectability and prebiotic organic delivery, here we present the results of an experiment using the dust accelerator and gas target facility at the University of Colorado to extend the study of the ablation process to particles with organic compositions. This facility has been used to study the basic physics of ablation. Past measurements included measuring the ionization efficiencies of Al and Fe particles (DeLuca et al., 2018; Thomas et al., 2016) and measuring the drag and heating of Al particles (DeLuca & Sternovsky, 2019). To extend such studies to more complex compositions, we used organic-coated particles in the present study. By using organic-coated particles, this study is complementary to studies of organic pyrolysis inside particles (e.g., Riebe et al., 2020). By shooting the organic-coated projectiles into a gas target and measuring their charge production, we studied the differential ablation of organics from micrometeoroids, constraining how and where organics undergo ablation in the atmosphere.

2. Experiment Design

We used the University of Colorado's dust accelerator and gas target facility to simulate the meteoric entry of organic-coated particles. The accelerator, which is described in detail by Shu et al. (2012), employs a Pelletron to generate voltages up to 3 MV that are used to accelerate charged particles from the accelerator's dust source. As each particle travels down the accelerator's beamline, image charge detectors measure its charge, mass, and velocity (Thomas et al., 2013). The accelerator typically shoots particles with radii from 10 nm to 1 μm at speeds up to 100 km/s. Generally, smaller particles will reach higher speeds and vice versa.

When particles enter the gas target, they slow down, heat up, and ablate, producing charges that are collected along the ablation path. The gas target is described in detail by Thomas et al. (2017). It attaches to the end of the accelerator's beamline, where a two-stage differential pumping unit separates the ultrahigh vacuum beamline of the accelerator from the gas target. The gas target can be backfilled with gases to pressures up to about 500 mTorr. The gas pressures are such that when particles from the accelerator enter the target, they ablate in free molecular flow, the flow condition that dominates for most of the mass influx to Earth. Atoms and molecules ablated from the particles strike gas molecules and produce ion-electron pairs that are collected on a series of 16 biased charge collectors arrayed along the beamline inside the target. The collectors are typically biased at 70–100 V to collect either ions or electrons. Each of these collectors is 26 mm long in the direction down the gas target to spatially resolve the charge production. The typical noise of the charge collector electronics corresponds to about 8,800 electrons. Those particles that did not completely ablate hit an impact detector located at the end of the gas target, approximately 47 cm from the entrance, and produced an impact charge signal. The signals from the 16 charge collectors and the impact detector provide spatially resolved measurements of the charge production by the particles as they traverse the gas, allowing their ablation to be studied under similar physical conditions as real meteors.

To study the differential ablation of organics, we used a bespoke synthetic mimic for dust particles comprising ground-up olivine particles coated in a thin layer of polypyrrole (PPy). PPy is a well-known organic-conducting polymer consisting of multiple pyrrole (C_4H_3N) repeat units linked together to form a conjugated backbone. On average, there is one cationic charge delocalized over every three or four pyrrole rings, so additional hydrogen sulphate (HSO_4^-) anions are incorporated between the cationic PPy chains to preserve electrical neutrality. The electrically conductive nature of PPy enables the PPy-coated particles to efficiently acquire surface charge, which is a prerequisite for their acceleration to hypervelocities using the dust accelerator. The olivine particles, which were sourced from San Carlos olivine, are primarily forsterite (Mg_2SiO_4). The olivine particles were coated with PPy using an aqueous deposition protocol described by Fielding et al. (2015); hypervelocity experiments using these particles were first reported by Li et al. (2014). Briefly, the pyrrole was polymerized using ammonium persulfate as an oxidant and the resulting insoluble PPy coats the olivine particles. The PPy mass loading on the final particles is 10.7%. The olivine particles have a rather ill-defined morphology (see Figure 1) but their sphere-equivalent particle radius prior to PPy deposition was 122 nm. Thus, the 10.7% PPy mass loading corresponds to a PPy overlayer thickness of approximately 10 nm. Such PPy-coated olivine particles can be efficiently charged within the accelerator's dust source and shot into the gas target at typical meteoric speeds.

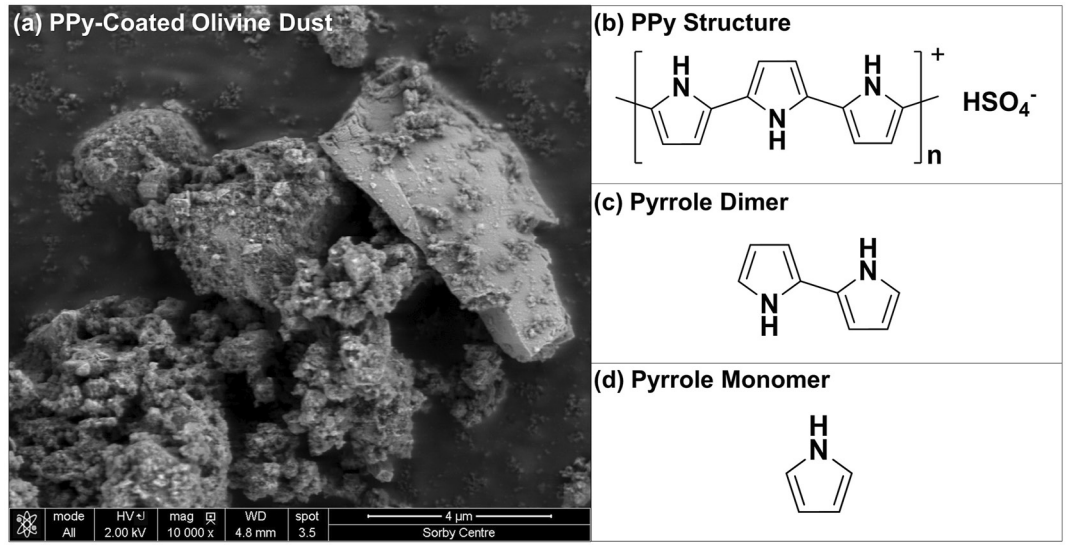

Figure 1. Figure showing the chemical structure of polypyrrole (PPy) as well as pyrrole monomer and dimer, which are potential large ablation products. Panel (a) shows a scanning electron microscope picture of the dust sample.

For this experiment, PPy-coated olivine particles were shot into the gas target, where they ablated and produced charges that were collected by the gas target's charge collectors. The gas target contained air at pressures of 30–100 mTorr for the experiments described. Approximately 100 particles were detected entering the gas target and ablating. These particles were shot across a wide speed range from 10 to 80 km/s. In this paper, we focus on 22 of these particles, which are mostly in the range of 10–20 km/s, which showed clear signs of differential ablation as described in the next section. When these 22 particles entered the target, differential ablation of the PPy surface coating and the particle interior occurred with enough separation to be spatially resolved by the charge collectors inside the target.

The experiment was designed to minimize potential biases in the charge measurements due to charge enhancement, charge spreading, and particle slowdown. In this experiment, the charge collectors were biased at 70 V to collect electrons, a bias level that ensures that charge enhancement due to electron impact ionization is minimal. At pressures of 100 mTorr and less, the enhancement should be under 15% at a bias voltage of 70 V (Thomas et al., 2017), so the electron impact enhancement is ignored here. Furthermore, as collisions between ablated molecules and the background gas cause ionization, there are some displacement and spatial spreading of the charges due to inertia. According to Thomas et al. (2017), the displacement and spreading of ions produced in such experiments are each on the order of 6–9 mm, which is small compared to the 26 mm width of the charge collectors. The displacement and spreading are limited to at most one or two collectors. We further mitigated the effect of displacement by biasing the charge collectors positively, that is, to collect negative charges, either in the form of free electrons or negative ions. Electrons have less inertia, thus on average, they will be collected closer to their creation point than ions. Finally, the particles decelerate during ablation, which could lower the ionization efficiency of the ablated molecules. However, the gas densities, particle sizes, and particle speeds used in this experiment were such that this deceleration is minimal, which we confirmed by the modeling presented in Section 4. In summary, there are no significant biases in the charge measurements.

3. Measurements

3.1. Initial Results

During the experiment, we observed that PPy-coated olivine particles enter the gas target and produce detectable charges through ablation and ionization. Out of the particles that produced detectable ionization, 22 particles exhibited ablation signals that may show differential ablation. For 18 of these 22 particles, a short but intense burst of charge production was observed like those shown in Figures 2b–2d prior to the particle striking the impact detector at the end of the gas target. Such signals appear to show the differential ablation of the PPy

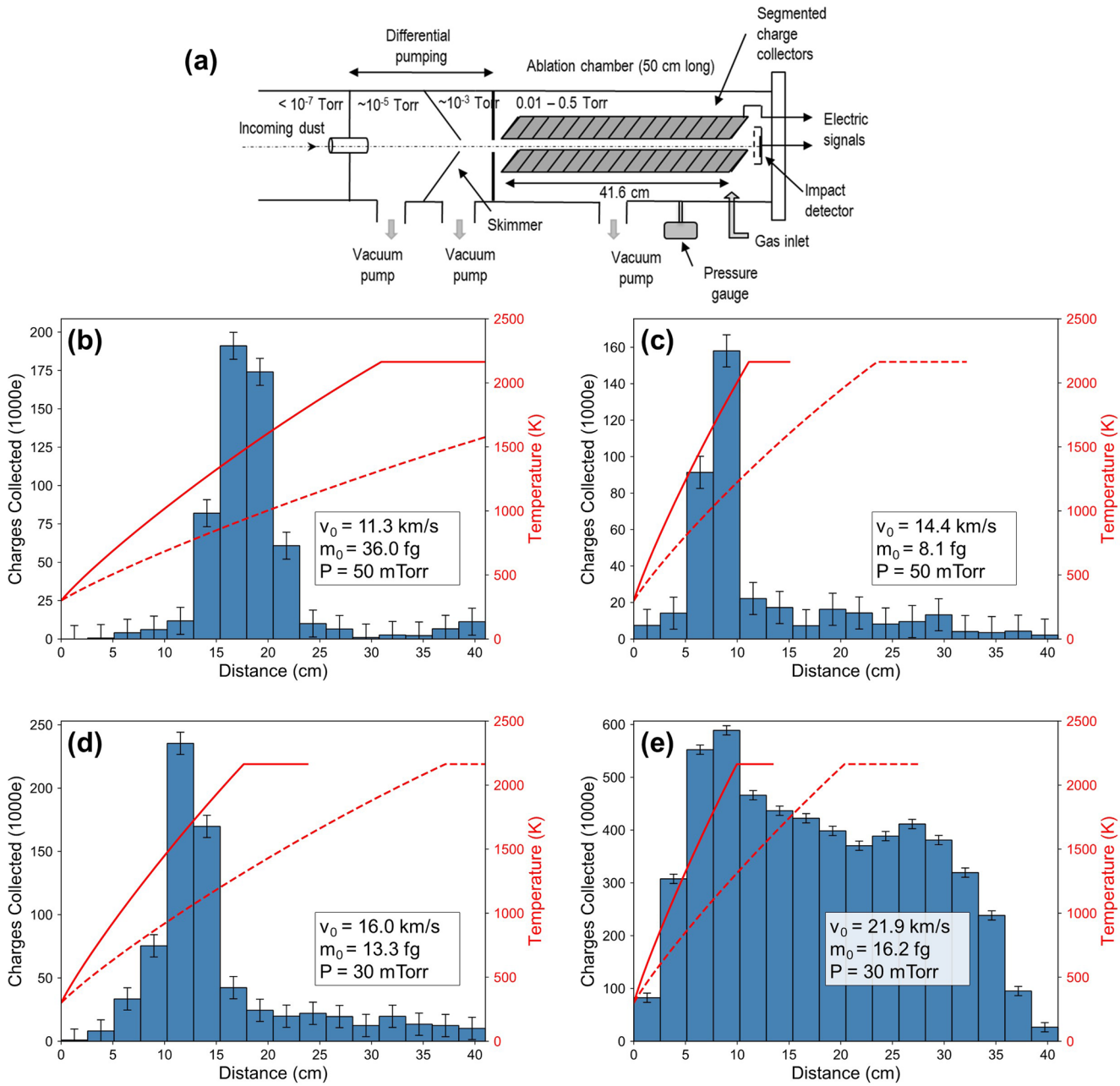

Figure 2. Schematic diagram of the gas target setup (not to scale, for more details, see Thomas et al., 2017) and 4 PPy-olivine ablation charge signals (in units of thousands of electrons) as a function of distance within the gas target. The particles moved from left to right and 0 cm mark the entrance aperture. Each column represents the total charge collected on the corresponding electrode with 2.6 cm width. Estimated temperature curves assuming that the particles are pure olivine for heating coefficients $\Lambda = 1$ (solid line) and $\Lambda = 0.5$ (dashed line) are plotted on the ablation profiles; the temperature curves stop when the particle has fully melted, which occurs at forsterite olivine's melting point of 1,890°C. Figures 2b–2d show just PPy ablation, while Figure 2e appears to show ablation of both PPy and olivine. The relevant parameters for each profile are shown in the figure. See text for more details.

coating from the particles: the ablating PPy causes the charge burst measured by the charge collectors, then the olivine core of the particle strikes the impact detector. The other 4 particles may exhibit olivine ablation as well as PPy ablation. In at least 2 of these 4 cases, the ablation profiles include an initial spike followed by a broad charge signal presumably from the olivine core, like that seen in Figure 2e. The particle in Figure 2e traveled somewhat faster than the others shown in Figure 2 and hence was more strongly heated, meaning that it surpassed the melting temperature of olivine (1,890°C for forsterite). Its profile shows that at sufficiently high speeds, the olivine will ablate. However, at lower speeds, only PPy might ablate.

A simple heating model shows that in most cases the ablation spikes occurred before the olivine cores could melt. We assumed that the particles were pure olivine spheres and calculated their temperatures using the heating equation given in Vondrak et al. (2008). The PPy coating was neglected at this stage, and so was mass loss; therefore, we stopped the calculation after the particles had fully melted (we present a more sophisticated model in Section 4). We ran the calculations for both high and low heating coefficients ($\Lambda = 1$ and $\Lambda = 0.5$) for each of the signals in Figure 2. Λ is the heating coefficient, the fraction of kinetic energy absorbed by the particle, which can be between 0 and 1. In Figures 2b–2d, the ablation pulses occur before the olivine has melted, which indicates that the observed ablation is not from this inorganic component. In Figure 2e, the particle is heated to temperatures above the melting point of olivine soon after entering the gas target. Accordingly, both PPy (the initial sharp charge signal) and olivine (the subsequent broad charge signal) appear to ablate. This simple model therefore suggests that most of the observed charge pulses are from the organic coatings.

Indeed, the PPy overlayer should ablate prior to the olivine core because the PPy is more thermally fragile, and the simple heating model shows that olivine cannot be responsible for the observed ablation. There is no evidence of sputtering, which would produce a steady level of charge production once a particle enters the gas target. Moreover, the limited duration of the charge pulses indicates that the PPy coatings on the particles are completely ablated. These observations may be used to constrain how PPy ablates. In the following sections, we use the 18 PPy ablation events where only PPy ablation was observed to constrain its ablation.

3.2. Threshold Velocity Constraints on Ion Production

To identify which molecules could be responsible for the observed charge production during PPy ablation, we calculated the threshold velocities required to ionize various atoms and molecules in air. Our results demonstrate that large organic molecules are the most likely source for the observed charges. The threshold velocity for ionization in head-on collisions of molecular or atomic species i is defined by

$$v_{0,i} = \sqrt{\frac{2\,(M_i + M_{gas})\,E_i}{M_i M_{gas}}} \tag{1}$$

where M_i is the molecular mass of the ablated species, M_{gas} is the molecular mass of the gas molecule, and E_i is the ionization energy of species i (all SI units). Note that E_i may be replaced with E_{gas} if the ionization energy of the gas is lower than the ionization energy of the molecular species. The threshold velocity is the minimum value required to ionize either the gas or the ablated molecule. Comparing threshold velocities to particle velocities constrains the sources of the observed ionization because many candidate molecules can be ruled out as sources. If the threshold velocity to ionize a molecule is higher than the speed at which a particle was shot into air, then that molecule cannot be responsible for the observed charge production by that particle.

Table 1 shows the threshold velocities in N_2 and O_2 for various possible products of PPy ablation. Many of these products are from Lifshitz et al. (1989), who studied the decomposition of pyrrole at high temperatures in a shock tube. The final column in Table 1 shows the number of PPy ablation events (out of 18 for which only PPy ablation was observed) observed above each molecule's threshold velocity. For example, pyrrole could potentially explain all 18 of the PPy charge signals, while ethane could only explain 10 of them.

Since charge production is observed at velocities as low as 10.5 km/s, many small ablation products are ruled out as potential sources of the observed ionization. For example, pure C has threshold velocities in N_2 and O_2 that are too high to explain the observed ionization in most cases. Likewise, CH_4 and HCN can be ruled out. Instead, larger organic molecules in Table 1 have both the high masses and low ionization energies that are required to explain the observed ionization at low speeds. That is not to say that small molecules, such as C, CH_4, or HCN, do not ablate, but they cannot produce ions at the lowest speeds, meaning that molecules with lower threshold velocities must also ablate in significant amounts. Since lower threshold velocities favor larger molecules, this suggests that such species are responsible for the observed ionization.

3.3. Charge Yield Constraints on Ion Production

We further constrain the ablation products of the PPy coating by calculating the charge yields of the coatings in air (for impact charge yields of PPy, see Burchell et al., 2002 and Goldsworthy et al., 2003). The measured yields

Table 1
Summary of Potential PPy Ablation Products With Their Corresponding Threshold Velocities v_0 in O_2 and N_2

Molecule	Ionization energy (eV)	Mass (u)	v_0 in O_2 (km/s)	v_0 in N_2 (km/s)	# Above v_0 in O_2
C_4H_5N (Pyrrole)	8.21	67	8.55	8.96	18
C_4H_5N (3-Butenenitrile)	10.20	67	9.53	9.98	18
C_4H_3N (Cyanoallene)	10.1	65	9.53	9.98	18
C_3H_3 (Propargyl Radical)	8.68	39	9.76	10.14	18
C_3H_2O (2-Propynal)	10.70	54	10.14	10.58	18
C_3H_4 (Allene)	9.69	40	10.25	10.65	18
C_3H_3N (2-Propenenitrile)	10.91	53	10.27	10.72	18
SO_2	12.35	64	10.45[a]	11.06	18
C_3H_4 (Propyne)	10.36	40	10.60	11.01	17
C_3H_5N (Propanenitrile)	11.85	55	10.63	11.10	17
C_3HN (Propiolonitrile)	11.62	51	10.68	11.14	17
CO_2	13.78	44	11.21[a]	12.46	13
C_2H_3N (Acetonitrile)	12.20	41	11.38[a]	11.89	11
C_2H_4 (Ethylene)	10.51	28	11.65	12.04	11
C_2H_6 (Ethane)	11.52	30	11.97	12.38	10
O_2	12.07	32	12.07	12.49	10
C_2H_2 (Acetylene)	11.40	26	12.38	12.77	9
N_2	15.58	28	12.49[a]	14.65	9
CO	14.01	28	12.49[a]	13.90	9
HCN	13.60	27	12.61[a]	13.81	7
NH_3	10.07	17	13.22	13.55	6
H_2O	12.62	18	14.22[a]	14.91	5
CH_4	12.61	16	14.78[a]	15.46	3
O	13.62	16	14.78[a]	16.06	3
N	14.53	14	15.46[a]	17.33	2
C	11.26	12	15.77	16.08	2

Note. The final column provides the number of events (out of a total of 18 for which only PPy ablation was observed) with velocities above the threshold velocity of that molecule, which is a possible source of observable ions in those events. The ionization energies are from Lias (2021).

[a]In cases marked with an asterisk, the threshold velocity for ionizing the gas molecule is lower than the threshold velocity for ionizing the ablated molecule. The lower threshold velocity is reported here.

are consistent with molecules whose mass is either comparable to or greater than that of pyrrole. To calculate the charge yields, we examined events for which a single, clear charge pulse was observed prior to impact. The sum of all charges from the individual collectors in the pulse gives the total charge Q_{pulse} produced by the ablation and ionization of the coating. We included only those collectors that measured a charge above a threshold set at 15,000 electrons. This threshold value ensures that the signal is clearly above the noise level of the electronics after smoothing the data. On average, a typical particle comprises approximately 10.7% PPy, so we can calculate the mass of PPy on each particle from its total mass. The charge yield of the PPy coating is then

$$Y = \frac{Q_{pulse}}{m_{PPy}} = \frac{Q_{pulse}}{0.107 m_0} \tag{2}$$

where $m_{PPy} = 0.107 m_0$ is the mass of PPy on a particle of initial mass m_0. In practice, there will be some variations in m_{PPy} for each particle, which inevitably lead to some scatter in the calculated yields. The errors in the calculation of Y depend on the uncertainty in the mass determination and the error in the number of collected charges. The noise on each collector is typically 8,800 electrons, and the error in mass determination is about

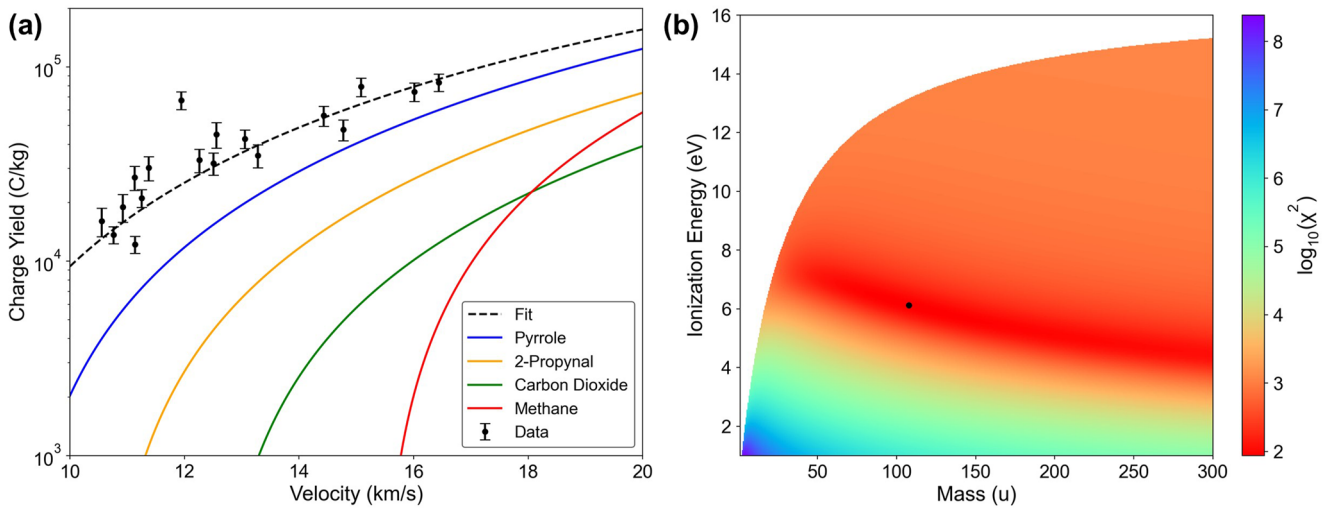

Figure 3. (a) The charge yield produced from the ablation of the PPy coating in air. The dashed curve shows the best fit to Equation (6). The solid curves show the estimated charge yields of various compounds that may be generated during ablation. (b) Solution space to the charge yield curve fit using Equation (7). The black point shows the best fit, but a range of solutions with high mass or low ionization energy could give suitable results. Some combinations of E_i and M_i are not physically realistic as they lead to threshold velocities faster than the speeds of the slowest particles; these solutions are shown as whitespace in the figure.

10%, resulting in a total error on Y of 10%–20% for each of the charge yields calculated here. The results are shown in Figure 3 as a function of velocity.

The chemical species produced by PPy ablation can be constrained by comparing the data to theoretical yields. In general, the charge yield is given by

$$Y(v) = \sum_i \frac{\beta_i n_i e}{M_{Py}} \tag{3}$$

where the sum is over all species i produced during PPy ablation. β_i is the ionization efficiency of molecule i in air, M_{Py} is the molecular mass of pyrrole, and n_i is the number of molecules of species i produced per molecule of pyrrole. For example, if the PPy coating completely degraded into its individual C atoms, then we would have $n_C = 4$ because there are 4 C atoms within each pyrrole repeat unit. To estimate β_i, we used the equation for ionization efficiency presented in DeLuca et al. (2018):

$$\beta_i(v) = \frac{c_i(v - v_{0,i})^{1.6} v^{0.8}}{1 + c_i(v - v_{0,i})^{1.6} v^{0.8}} \tag{4}$$

where $v_{0,i}$ is the threshold velocity of species i (see Equation (1)) and c_i is a parameter specific to species i. Janches et al. (2017) provided the following formula to estimate c_i by scaling it to c_{Fe} for iron:

$$c_i = c_{Fe}\left(\frac{E_{Fe}}{E_i}\right)^2. \tag{5}$$

Although Equation (5) was developed for metal atoms, it is applied to nonmetals here in order to estimate c_i, which is unknown for organic molecules. We used an average value of v_0 and c for air rather than adding the contributions from O_2 and N_2 separately, as measurements of c_{Fe} in air are more readily available (e.g., DeLuca et al., 2018; Thomas et al., 2016). These approximations allow us to estimate the ionization efficiency and the charge yield curves for various products that may be produced during ablation.

However, simplifying assumptions are required to make the problem tractable. To simplify Equation (3), we assumed that only one type of molecule produces ions, and that the PPy coatings completely transform into that molecule. The assumption that only one molecule produces ions removes the summation in equation (3), while the assumption that the PPy coatings completely transform into that molecule allows us to replace M_{Py}/n_i by M_i, the molecular mass of the ablated molecule. Equation (3) then becomes

$$Y = \frac{\beta_i e}{M_i} \tag{6}$$

where i is now the single unknown ablated species. The remaining unknowns in Y are the molecular mass M_i of the ablated molecule and its ionization energy E_i. These can be varied to determine the best fit to the data.

By fitting $Y(v)$ to the charge yield measurements and comparing the measurements to estimated curves for possible ablation products, we find that the data are consistent with relatively large molecules ablating from the PPy coating. We determined the best fit by minimizing the sum of the squared differences between the model and the 18 data points Y_i at speeds v_i with each point weighted by its uncertainty δY_i:

$$\chi^2 = \sum_{i=1}^{18} \left(\frac{Y(v_i) - Y_i}{\delta Y_i} \right)^2. \tag{7}$$

The best fit occurs at $M_i = 108$ u and $E_i = 6.1$ eV, which is shown in Figure 3a. These values correspond to a threshold velocity of 7.2 km/s and a c parameter of 3.3×10^{-4} (s/km)$^{2.4}$ using Equations (1) and (5). However, this result does not necessarily prove that those are the actual molecular mass and ionization energy of the ablated molecules. Instead, it simply indicates that they fit the data best, given the simplified model presented above. A range of masses and ionization energies is also consistent with the data. Figure 3b shows the solution space to Equation (7), and acceptable solutions may be found for masses greater than 50 u that all share the property of having relatively large masses and low ionization energies. The results suggest that the PPy ablates to form relatively large organic molecular fragments. The fragments may include two or more pyrrole rings, for example, the dimer in Figure 1c, since the best-fit mass is greater than the mass of a single polymerized pyrrole repeat unit (65 u). This is physically reasonable because the C-C aliphatic bonds between the polymerized pyrrole repeat units are weaker than the C-C and C-N bonds within the aromatic pyrrole rings; hence, the former are more readily cleaved. These findings are consistent with the threshold velocity constraints reported in Table 1, which suggest that only relatively large molecules can explain the observed charge production. However, that table is limited to known molecules with masses no greater than that of pyrrole although the fit here suggests that larger organic fragments may be responsible for the observed ionization yield. In any event, the ablation products appear to be relatively large organic molecules.

Figure 3a also shows other theoretical charge yields, including that calculated for pure pyrrole for comparison to the measurements. These theoretical yields were calculated using Equation (6): this assumes that the PPy completely transforms into the target molecule, which is likely to overestimate the true yield. The theoretical yield for pyrrole more closely resembles the measured charge yields than those calculated for alternative smaller molecules. However, these theoretical charge yields should only be regarded as rough estimates, since the ionization efficiencies of pyrrole and other organic molecules are unknown and have to be estimated using Equation (5). This ultimately limits our ability to identify the ions produced in the experiment. Nevertheless, it appears that large organic fragments comparable in mass to pyrrole or its oligomers are consistent with the experimental observations.

4. PPy Ablation Model

We can model the ablation and mass loss of the PPy coating, which demonstrates that the differential ablation of organics can be described using a simple physical model and is also useful for constraining the heating process. We fit a two-component ablation model to the observed PPy charge profiles consisting of spherical olivine particles coated in a PPy overlayer. This model can adequately explain the PPy ablation and also provides constraints on the heating coefficient.

The model is based on that by Vondrak et al. (2008), uses the Arrhenius equation, and includes heating of the particle by gas molecule impacts and ablation of the PPy coating. To model PPy ablation, we assumed that this component degrades to form pyrrole. We chose pyrrole as the ablation product because it is roughly consistent with the threshold velocity constraints and charge yield data discussed in Sections 3.2 and 3.3. Although some of the ablation products may be larger than pyrrole, we still choose pyrrole here because its thermodynamic properties are known, unlike those of larger fragments, such as pyrrole dimer. We assume that the pyrrole molecules are immediately volatilized after being generated as the particles rapidly reached temperatures well above the boiling

point of pyrrole (129°C). We used the Arrhenius equation to describe the reaction rate for the thermal decomposition of PPy, and we assume that this reaction proceeds with first-order kinetics, meaning that the degradation rate of PPy is proportional to its concentration. Using the Arrhenius equation, the reaction rate constant k is given by

$$k(T) = A \exp\left(-\frac{E_a}{N_A k_B T}\right) \tag{8}$$

where A is the pre-exponential factor for PPy degradation, E_a is the activation energy, N_A is Avogradro's number, k_B is Boltzmann's constant, and T is the temperature. Assuming a first-order reaction, the rate is given by

$$\frac{d[\mathrm{PPy}]}{dt} = -k(T)[\mathrm{PPy}] \tag{9}$$

where t is time and [PPy] is the concentration of PPy. Roughly equating the concentration of PPy with its mass density on the surface, we model the mass of PPy m_{PPY} remaining on the particle by

$$\frac{dm_{PPy}}{dt} = -Am_{PPy} \exp\left(-\frac{E_a}{N_A k_B T}\right). \tag{10}$$

The mass of pyrrole m_{Py} that is immediately volatilized after being released from the PPy chains is then related to PPy loss through

$$\frac{dm_{Py}}{dt} = -\frac{dm_{PPy}}{dt}. \tag{11}$$

The degradation of PPy increases strongly with temperature based on this model. Since we assume that the pyrrole immediately volatilizes once it is formed, the release of this molecule from the particle depends solely on the rate of decomposition of the PPy. Although there may be more sophisticated ways to describe PPy degradation, these equations provide a simple way to describe the PPy coating's mass loss.

We model PPy ablation by combining the mass loss portion of the model with a meteoric heating model. The heating model is based on the general meteoric heating equation (as given by Vondrak et al., 2008), which is refined here to model a particle with an inner and outer layer made of different materials. The olivine particles used in the experiment are mostly forsterite (Mg_2SiO_4), so we used forsterite's thermal properties in the model. Assuming spherical particles, the energy balance is given by

$$\frac{\pi}{2} R^2 v^3 \rho_{air} \Lambda = 4\pi R^2 \epsilon \sigma \left(T^4 - T_{env}^4\right) + \left(m_{fo} C_{fo} + m_{PPy} C_{PPy}\right) \frac{dT}{dt} + \left(L_{\mathrm{Py}} + E_a\right) \frac{dm_{Py}}{dt} \tag{12}$$

where v is the particle's velocity through the gas, ρ_{air} is the air density, R is the total radius of the particle (including both the olivine core and the PPy coating), ϵ is the emissivity of the particle (assumed to be equal to unity), T_{env} is the ambient temperature, σ is the Stefan-Boltzmann constant, m_{fo} is the mass of forsterite olivine, C_{fo} is the specific heat capacity of forsterite, C_{PPy} is the specific heat capacity of PPy, L_{Py} is the latent heat of pyrrole, and Λ is the heating coefficient. This equation is similar to the heating equation in Vondrak et al. (2008), but the second and third terms on the right have been modified to account for the PPy coating and its breakdown. The term on the left describes the kinetic energy input to the particle. The first term on the right describes the radiative emission from the particle. The second term on the right describes the temperature rise of the particle by combining the heat capacities of both the olivine core and the PPy coating. The third and final term on the right describes the energy loss due to mass loss. There are two steps to the mass loss as described above: first, the PPy degrades to form pyrrole, and then the pyrrole is volatilized. The energy required to convert PPy into pyrrole is assumed to be E_a, the activation energy used in Equation (8), and the energy to volatilize the pyrrole is the latent heat of pyrrole L_{Py}, so the total energy required to vapourize a unit mass of PPy is the sum of these two components.

In addition to heating, the particle also decelerates. Slowdown is a minor effect for the particles in this experiment owing to the low pressures used in the gas target, but it is nonetheless included here for completeness. This effect was modeled using the free molecular drag equation for a sphere given by

$$\frac{dv}{dt} = -\Gamma \frac{3\rho_{gas}}{4\rho_{avg} R} v^2 \tag{13}$$

where Γ is the drag coefficient and ρ_{avg} is the average particle density. Since the particles used in this experiment are a combination of two different materials, the average density of the particle is given by

$$\rho_{avg} = \frac{m_{fo}\rho_{fo} + m_{PPy}\rho_{PPy}}{m_{fo} + m_{PPy}} \tag{14}$$

where ρ_{fo} and ρ_{PPy} are the densities of forsterite olivine and PPy, respectively. The drag coefficient Γ and the heating coefficient Λ are connected by conservation of energy and momentum. Assuming that gas molecules reflect diffusely from the particle surfaces, the relationship between drag and heating is given by

$$\Gamma = 1 + \frac{4}{9}\sqrt{1 - \Lambda} \tag{15}$$

(Cook, 1965). With the drag coefficient depending on the heating coefficient, we can now model the ablation of the PPy coatings on the particles. The values of A, E_a, and Λ are parameters that can be fit to the data. A and E_a relate to the breakdown of PPy, while Λ describes the energy transfer from the gas to the particle.

We fit the two-component model described above to the observed PPy ablation profiles. To reduce the number of free parameters in the model, we fixed $E_a = 350$ kJ/mol, which is the approximate energy required to break a single aliphatic C–C bond. This value for E_a is a rough estimate based on the fact that many C–C bond dissociation energies in polyatomic hydrocarbons are approximately in the range of 300–400 kJ/mol (Luo & Cheng, 2019). By fixing E_a at that value, we are assuming that the PPy degrades via random cleavage of the relatively weak aliphatic C–C bonds between pyrrole rings. With E_a fixed, only A and Λ remain to be fit by the model.

Before fitting the data, we converted the observed PPy ablation profiles into the fraction of PPy remaining on each particle. Since the model output is the PPy mass m_{PPy} remaining on the particle, it is easier to fit the model to the data when framed in this manner. To determine the quantity of PPy remaining on the particle, we assumed that the fraction of PPy on the particle is 1 prior to the ablation pulse and 0 after the ablation pulse has fallen below a noise threshold set at 15,000 electrons. The ablation pulse is defined to be located where the number of charges per collector exceeds the noise threshold. The fraction of PPy remaining on a particle after passing the end of charge collector i is given by

$$F_i = 1 - \frac{q_1 + q_2 + \ldots + q_i}{Q_{pulse}} \tag{16}$$

where the numerator contains the total number of charges acquired by the collectors up to and including collector i, and Q_{pulse} is the total number of charges collected during the full ablation pulse. q_i is taken to be 0 if it is below the 15,000 electron measurement thresholds. Using Equation (16), we converted the PPy ablation profiles into the fraction of PPy remaining on each particle; Figures 4a and 4b shows an example.

We fit all 18 PPy ablation events simultaneously to determine the best values of A and Λ compared to the data. We determined the goodness of the fit by summing the weighted squared differences between the observed PPy fractions and the model. If F_i is the observed fraction of PPy remaining after the particle passes collector i, and $F(x_i)$ is the modeled PPy fraction at point x_i (x_i is the farthest extent of collector i down the beamline of the gas target), then the goodness of fit for event j is given by

$$\chi_j^2 = \sum_{i=1}^{16} \left(\frac{F(x_i) - F_i}{\delta F_i} \right)^2. \tag{17}$$

The goodness of fit for all 18 observed events is then the sum of Equation (17) for all events:

$$\chi^2 = \sum_{j=1}^{18} \chi_j^2. \tag{18}$$

we found the best fit between the model and the data by minimizing Equation (18).

The best fit between the model and the data occurs when there are moderate levels of heating although the final results are consistent with a range of possible values of A and Λ. The best fit occurs when $\Lambda = 0.71$ and $A = 10^{21.8}$ s^{-1}. Figure 4 shows an example of an observed event compared to the model using these parameters. The best-fit

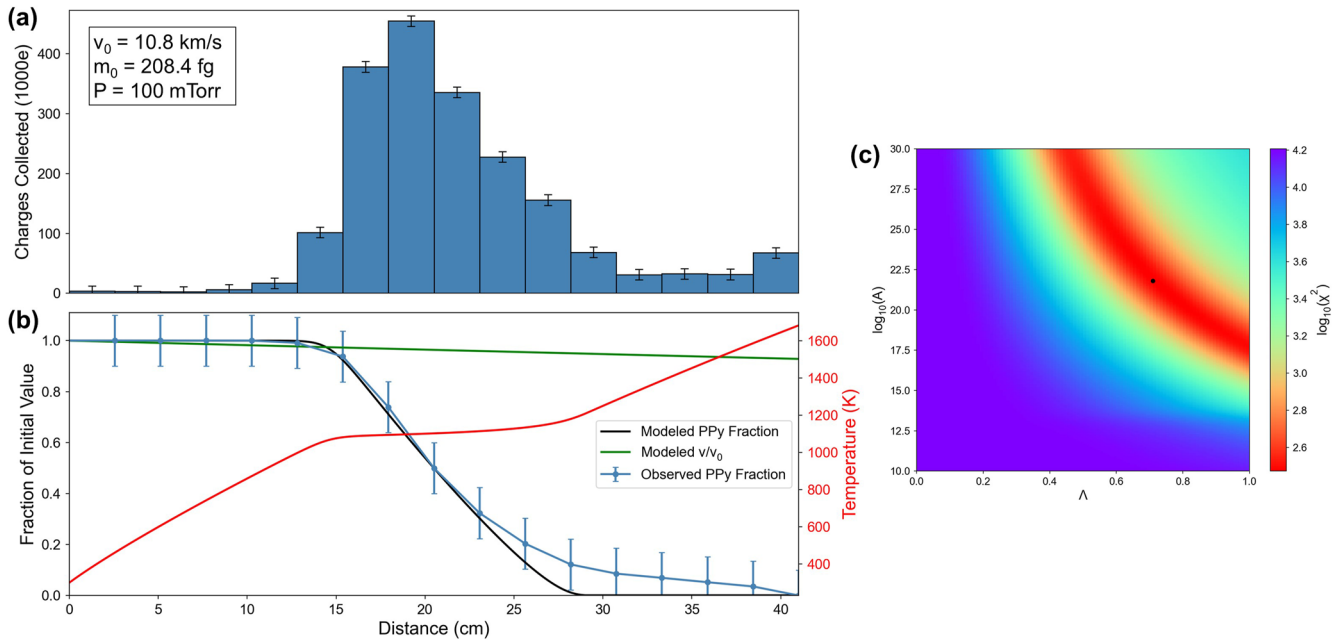

Figure 4. (a) and (b) Comparison between observed and modeled PPy ablation for an event with a good match between the observations and the model. The top panel shows the observed charge profile (in units of thousands of electrons). The bottom panel shows the observed fraction of PPy remaining on the particle, determined using Equation (16), compared to the remaining PPy fraction, velocity, and temperature output by the model. (c) Solution space of the fit between the ablation model and the 18 events for different values of parameter A (in units of s^{-1}) and the heating coefficient Λ using Equation (18). The black point shows the best fit.

heating coefficient is consistent with the results of DeLuca and Sternovsky (2019), who found that the heating coefficient can be less than 1. Using Equation (15), the best-fit heating coefficient corresponds to a drag coefficient $\Gamma = 1.24$, which is very similar to the drag coefficients measured by DeLuca and Sternovsky (2019). However, a range of possible solutions to the model may also be consistent with the observations as shown in Figure 4c. For example, we cannot rule out $\Lambda \approx 1$ and $A \approx 10^{18}$ s^{-1} as a potential solution. Lower values of A would be consistent with the results of Lifshitz et al. (1989), who found $A = 10^{15.9}$ s^{-1} for the complete decomposition of pyrrole. However, since we assumed that PPy degrades to form pyrrole and that the pyrrole itself does not break down any further, it is not clear that A should be the same. Regardless of the precise values of the model parameters, our simple model provides a satisfactory description of PPy ablation.

5. Discussion and Conclusions

5.1. Discussion on Experimental Results

The experiments presented here demonstrate that organics can differentially ablate from the surfaces of micrometeoroids. The PPy coating ablated in a form most likely consisting of relatively large organic molecules. We successfully modeled this ablation by invoking basic meteor physics and a simple description of PPy decomposition into volatile pyrrole molecules. More complicated models may be possible, but our simple model is capable of fitting the measurements. These results are important because the survival of organic molecules during ablation may affect the inventory of organics available on planetary bodies. Organics may also affect the detectability of meteors by radar by causing bursts of electron production during atmospheric entry.

The survival of large organics during ablation is consistent with the expected chemistry at the high temperatures and fast speeds of ablating micrometeoroids. The particles in the experiment thermally ablate into what is effectively a vacuum. They are also flash-heated on time scales of tens of microseconds. Therefore, the decomposition and ablation of the PPy coating must be understood within the context of this elusive regime. Prior studies of the degradation of PPy on short timescales and at high temperatures are limited, but some useful information can be gleaned from other experiments. For example, Goldsworthy et al. (2003) found that large organic cations can survive hypervelocity impacts. Hillier et al. (2014) shot PPy-coated pyrrhotite onto an Ag target and observed the formation of complex organic anions and cations, including pyrrole and large fragments and clusters that

originated from the coating. Likewise, Srama et al. (2009) shot PPy-coated organic grains onto Ag and observed both aliphatic and aromatic ions that survived impact. However, distinct PPy features were not identified in that experiment, most likely because this component comprised less than 10% of the overall organic dust mass. These experiments show that complex organic molecules, including pyrrole, can survive the short heating durations and high energies that typify a hypervelocity impact. In addition, the decomposition of pyrrole at high temperatures was studied by Lifshitz et al. (1989) using a shock tube. Various degradation products were identified, including several isomers of C_4H_5N and a number of different hydrocarbons, many of which are included in Table 1. Although these prior experiments were conducted in different physical regimes than those experienced during meteor ablation, they confirm that complex organics can survive energetic heating processes on short timescales.

In addition, oxidation products can be ruled out as a significant ion source due to the low levels of O_2 inside the gas target. Although the particles traversed air, the relatively low pressures within the gas target mean that a typical particle only encountered 1 O_2 molecule for every 5 pyrrole repeat units in its coating. Also, the O_2 molecules were only present on the PPy surface for a short period of time due to their high incoming and recoil velocities. The low number of O_2 molecules encountering the surface and their high speeds makes it unlikely that oxidation plays a significant role during the ablation process. Even if CO_2 is produced by reactions between PPy and O_2, its threshold velocity (11.2 km/s in O_2) is too high to explain the charge production observed in all events. Likewise, SO_2, which may form from HSO_4^- in the PPy coating and has a relatively low threshold velocity, is unlikely to produce significant quantities of charged species. This is because there is only one HSO_4^- anion per 3–4 pyrrole repeat units, and the estimated charge yield of SO_2 is mostly below that of CO_2 in Figure 3 when the number of S atoms is taken into account. We conclude that neither SO_2 nor CO_2 is likely to affect the results.

In principle, the HSO_4^- anions within the PPy coatings could bias the charge measurements if the anions were released from the coatings while still holding a charge although we believe that this process is unlikely to produce a significant bias. Release of HSO_4^- anions would produce charge production by means other than ionization of neutrals through collisions with gas molecules, thereby undermining the ablation product constraints placed in Sections 3.2 and 3.3. However, we believe that the release of HSO_4^- anions is likely to be insignificant for two reasons: First, the measured charge yields are much lower than would be expected if all of the observed charges were simply due to HSO_4^- release. If the only charges collected in the gas target were HSO_4^- anions, and all HSO_4^- was released during ablation, the observed charge yield would be 3×10^5 C/kg, which is significantly higher than actually observed. Second, the measured charge yields increase with velocity. If solely released HSO_4^- was collected, the charge yields would remain constant with velocity, because the ratio of HSO_4^- to polymerized pyrrole repeat units remains constant. The increase in charge yield with velocity indicates that the ionization process is velocity-dependent, meaning that the ionization of ablated molecules by collisions with the gas most likely occurs. Although we cannot rule out HSO_4^- release as a source of observed charges in the experiment, we believe its influence is insignificant.

Given the threshold velocity constraints and the high charge yields, the simplest explanation for the data is that the PPy coatings degrade to form large organic fragments. These large organics then ablate from the particle into the gas. In our PPy ablation model, we assume that the aliphatic C-C bonds between pyrrole repeat units are cleaved. However, even if aromatic C-C and/or C-N bonds within the pyrrole molecules are also cleaved, large organic fragments may still be formed as found by Lifshitz et al. (1989). Small molecules simply do not have the large masses or low ionization energies to explain the production of ions and electrons at low meteoric speeds.

Finally, a notable aspect of the results for meteor detectability is that the organic coating produced a large charge yield. At 14 km/s, the charge yield of the organic coating is approximately 5×10^4 C/kg. Assuming that the source of the ionization is pyrrole molecules, that charge yield corresponds to an ionization efficiency $\beta \approx 3\%$, which is similar to those of Al and Fe at the same speed (DeLuca et al., 2018). This is a significant quantity of charge that may produce detectable amounts of plasma, especially since organics can be a large component of cometary dust.

5.2. Implications for Meteor Detectability

To explore the possibility that organics may affect meteor observations, we modeled an Fe particle coated in PPy ablating in the atmosphere and estimated the detectability of its head echo. We chose Fe because it is easy to model and its ionization efficiency has been determined in past experiments (Thomas et al., 2016; DeLuca et al., 2018). We combined the model described in Section 4 with an atmospheric density profile to model

ablation in Earth's atmosphere. The PPy coating ablated according to Equations (10) and (11), and the Fe core of the particle ablated via Langmuir evaporation (following Vondrak et al., 2008). Due to the lower heating rate, the differential ablation of the organics would occur at somewhat lower temperatures and over longer timescales. We used the NRLMSISE-00 empirical model (Picone et al., 2002) to simulate Earth's atmosphere.

We estimated the radar detectability of the particle by combining the modeled mass loss with a detectability model for meteor head echoes. We calculated the number of electrons produced per unit altitude by combining the modeled mass loss rate with the ionization efficiency of Fe and the charge yield of PPy. The ionization efficiency of Fe comes from DeLuca et al. (2018) using Equation (4), and the charge yield of PPy comes from the best-fit charge yield curve in Section 3.3, assuming that all of the produced charges are free electrons detectable by radar. We combined that with a radar detectability model based on Janches et al. (2017), in which the number of free electrons N_e produced by an ablating meteoroid and the mean free path A at the ablation altitude enables the radar cross section of the meteor head echo to be calculated with

$$\sigma = 4\pi(N_e r_e \ell F)^2 \tag{19}$$

(based on Mathews et al., 1997) where r_e is the electron radius. F is a factor defined by $F = 1$ when $\ell < \lambda/4$ and by $F = \lambda^2/\left(16\ell^2\right)$ when $\ell > \lambda/4$ (Janches et al., 2017; Swarnalingam et al., 2019). Here, we use the wavelength of the Arecibo 430 MHz radar. The radar cross-section can be used to estimate the signal-to-noise ratio (SNR) of the micrometeoroid. The SNR of a radar meteor is given by

$$\mathrm{SNR} = \frac{P_t \lambda^2 G^2 \sigma}{(4\pi)^3 P_n R^4} \tag{20}$$

where R is the range to the meteor, assumed here to be equal to altitude, λ is the radar wavelength, G is the gain of the antenna (assuming that the same antenna is used to both transmit and receive the radar signal), P_t is the transmit power, and P_n is the noise power. Assuming that the micrometeoroid ablates entirely above the same portion of the radar beam, that is, that G is constant over the meteor's ablation path, the SNR depends only on the radar cross section and the altitude of the meteor:

$$\mathrm{SNR} \propto \frac{\sigma}{R^4}. \tag{21}$$

To compare the SNR of the meteor during ablation of its organic coating with the SNR during ablation of its metallic core, we normalized the SNR of the meteor to the peak SNR during Fe ablation. Therefore, when the PPy coating ablates, a normalized SNR greater than 1 indicates that it is more detectable than the Fe core of the particle, and a normalized SNR less than 1 indicates that it is less detectable.

This model reveals that the organic coating may produce detectable amounts of charges relative to the Fe core depending how much organic material is present on the surface of the micrometeoroid. As a case study to illustrate organic ablation, Figure 5 shows the ablation of a hypothetical Fe particle coated in PPy entering Earth's atmosphere at 15 km/s. The particle consists of a core of 10 μg Fe surrounded by a 0.01 μg PPy layer, which corresponds to an approximate coating thickness of 120 nm on an Fe particle of 67 μm radius. This assumption is consistent with the findings of Flynn et al. (2013), who found organic coatings of approximately 100 nm thickness on the individual submicron grains that form micron-size aggregate particles. The particle entered the atmosphere at an angle of 0° to the zenith, and the heating coefficient was set to $\Lambda = 0.6$, which was the heating coefficient found by DeLuca and Sternovsky (2019). The ablating particle deposited its entire PPy content into the atmosphere over a relatively narrow altitude range of 93–94 km. About 70% of the Fe core of the original particle ablated with maximum Fe ablation occurring at approximately 78 km. The radar SNR of the particle peaked during Fe ablation. Nevertheless, there was a narrow but intense increase in SNR due to PPy ablation at 93–94 km with a peak about an order of magnitude lower than the peak during Fe ablation. The PPy on the simulated particle thus behaves similarly to Na and K in actual meteors, which produce narrow but intense spikes in head echo SNR prior to the ablation of the rest of the particle (e.g., Janches et al., 2009). The magnitude of the SNR due to PPy ablation depends strongly on the amount of PPy in the particle coating. For example, increasing the mass of the PPy coating from 0.1% to 1% of the Fe core mass increases the radar SNR due to PPy ablation by two orders of magnitude. This increase in SNR occurs because the radar cross-section σ scales as $\sigma \propto N_e^2$ during the relatively fast PPy ablation, where N_e is the number of electrons produced by the coating. Such an increase

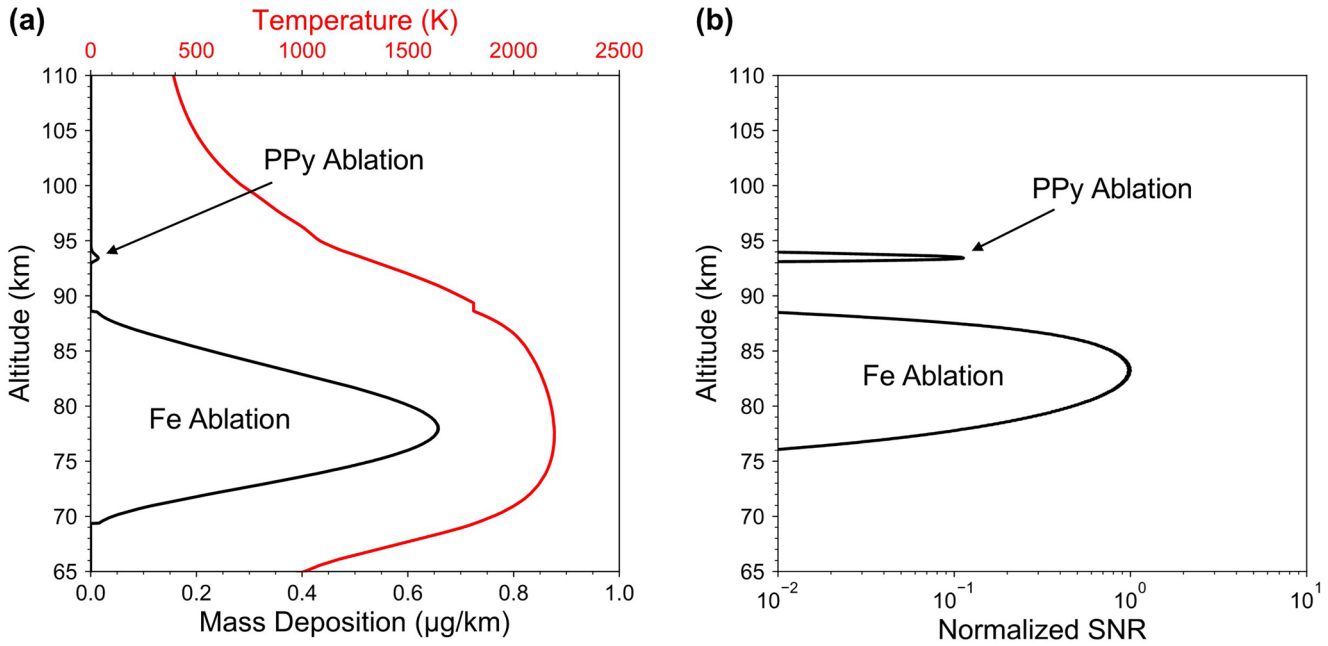

Figure 5. Ablation of a hypothetical PPy-coated Fe particle in Earth's atmosphere. The particle consists of a 10-μg Fe core coated in 0.01 μg PPy and entered the atmosphere at 15 km/s. The PPy ablates around 93–94 km, while the Fe ablation peaks at 78 km. The SNR is normalized to the peak SNR of the Fe ablation. Only 70% of the Fe component of the original particle ablates, meaning that the remainder of the particle forms an organic-free micrometeorite.

in SNR would make the PPy ablation easier to detect than the Fe core ablation although the PPy ablates over a relatively narrow range of altitudes, whereas the Fe ablation has a much broader profile. This could potentially explain the existence of a high-altitude tail on the altitude distribution of meteors present in Arecibo observations (Swarnalingam et al., 2019).

In summary, the case study above indicates that organic coatings on micrometeoroids may increase the detectability of meteors at higher altitudes by radars. The detectability is enhanced due to the narrow altitude range over which the complex organics are deposited and the efficient ionization of these molecules. Realistic organic coatings on micrometeoroids, however, may consist of complex compounds with a range of activation energies. The consequence is then the ablation of organics over a wider altitude range, which in turn would reduce the detectability of the meteors in comparison with the homogenous organic coating considered in the case study.

5.3. Implications for Prebiotic Organic Delivery

Organic ablation from the surfaces of micrometeoroids could provide a pathway for the delivery of organics into the atmosphere, which may have contributed to the origin of life on Earth. For example, the hypothetical PPy-coated particle modeled in Figure 5 deposits its entire organic coating into the atmosphere at an altitude about 15 km above the peak in Fe ablation. Although the particle reaches a peak temperature over 2000 K, its organic component thermally ablates at much lower temperatures and thus higher altitudes. As shown in our experiments, the organic PPy coating appears to ablate as complex molecules that are not destroyed by ablation, which suggests that organics ablated during the atmospheric entry of real micrometeoroids could also survive. Our experiments are consistent with previous studies, including the finding by Glavin and Bada (2001) that glycine can survive sublimation from meteorites and studies by Jenniskens et al. (2000, 2004) which suggested that organics may survive meteoroid ablation.

The quantity of organics that micrometeoroids deposit into the atmosphere could be significant compared to the quantity delivered to Earth's surface by interplanetary dust particles, provided that the ablated organics survive exposure to the atmosphere. The vast majority of the incoming mass flux forms meteors; only a minor portion of the influx is sufficiently small enough to pass through the atmosphere intact. For example, Flynn et al. (2004) estimated that out of approximately 30,000 tons/year of incoming meteoric material, only 1%, or about 300

tons/year, are heated to temperatures below 600°C and can feasibly deliver their organics intact. The remaining 99% of incoming particles are too strongly heated to deliver organics to the surface. However, based on our laboratory experiments, those strongly heated particles may still contribute organics by ablating them directly into the atmosphere. Such organics would have to be present on the surfaces of the micrometeoroids or be exposed by fragmentation during atmospheric entry. The ablated organics would then have to survive transit through the atmosphere to Earth's surface in order to contribute to the prebiotic organic inventory. In particular, such organic molecules (or large fragments thereof) would have to survive hyperthermal collisions with gas molecules, dissociative recombination if they are ionized, exposure to ultraviolet radiation, and reactions with other species in the atmosphere. However, even if only a minor fraction of the organics in micrometeoroids survives, it could still rival the quantity delivered to the surface by small dust particles. Chyba and Sagan (1992) showed that small interplanetary dust particles may have delivered the dominant source of exogenous organics to Earth prior to the origin of life. If meteors also contributed intact organics, then their contribution to the early Earth's prebiotic organic inventory could have been similarly significant.

Data Availability Statement

The data presented in this article can be found in a repository (Sternovsky, 2022).

Acknowledgments
M. D. acknowledges that this material is based upon work supported by the National Science Foundation Graduate Research Fellowship Program under Grant No. DGE 1650115. Any opinions, findings, and conclusions or recommendations expressed in this material are those of the authors and do not necessarily reflect the views of the National Science Foundation. This research was also supported by NASA's Heliophysics Technology and Instrument Development for Science (HTIDeS) program, Grant No. NNX15AJ96G. The development of the gas target facility was supported by NASA's Solar System Exploration Research Virtual Institute (SSERVI): Institute for Modeling Plasma, Atmospheres, and Cosmic Dust (IMPACT), Grant. No. 80NSSC19M0217, and the National Science Foundation's Aeronomy program (Atmospheric and Geospace Sciences), Award No. 1451218. S.P.A. acknowledges EPSRC for providing a four-year *Established Career* Particle Technology Fellowship (EP/R003009).

References

Anders, E. (1989). Pre-biotic organic matter from comets and asteroids. *Nature*, *342*(6247), 255–257. https://doi.org/10.1038/342255a0

Bardyn, A., Baklouti, D., Cottin, H., Fray, N., Briois, C., Paquette, J., et al. (2017). Carbon-rich dust in comet 67P/Churyumov-Gerasimenko measured by COSIMA/Rosetta. *Monthly Notices of the Royal Astronomical Society*, *469*(S), S712–S722. https://doi.org/10.1093/mnras/stx2640

Bones, D. L., Gómez Martín, J. C., Empson, C. J., Carrillo-Sánchez, J. D., James, A. D., Conroy, T. P., & Plane, J. M. C. (2016). A novel instrument to measure differential ablation of meteorite samples and proxies: The Meteoric Ablation Simulator (MASI). *Review of Scientific Instruments*, *87*(9), 094504. https://doi.org/10.1063/1.4962751

Burchell, M. J., Willis, M. J., Armes, S. P., Khan, M. A., Percy, M. J., & Perruchot, C. (2002). Impact ionization experiments with low density conducting polymer-based micro-projectiles as analogues of solar system dusts. *Planetary and Space Science*, *50*(10–11), 1025–1035. https://doi.org/10.1016/S0032-0633(02)00071-5

Campbell-Brown, M. D., & Koschny, D. (2004). Model of the ablation of faint meteors. *Astronomy & Astrophysics*, *418*(2), 751–758. https://doi.org/10.1051/0004-6361:20041001-1

Carrillo-Sánchez, J. D., Gómez-Martín, J. C., Bones, D. L., Nesvorný, D., Pokorný, P., Benna, M., et al. (2020). Cosmic dust fluxes in the atmospheres of Earth, Mars, and Venus. *Icarus*, *335*, 113395. https://doi.org/10.1016/j.icarus.2019.113395

Carrillo-Sánchez, J. D., Nesvorný, D., Pokorný, P., Janches, D., & Plane, J. M. C. (2016). Sources of cosmic dust in the Earth's atmosphere. *Geophysical Research Letters*, *43*(23), 11979–11986. https://doi.org/10.1002/2016GL071697

Chyba, C., & Sagan, C. (1992). Endogenous production, exogenous delivery and impact-shock synthesis of organic molecules: An inventory for the origins of life. *Nature*, *355*(6356), 125–132. https://doi.org/10.1038/355125a0

Chyba, C. F., & Hand, K. P. (2006). Comets and prebiotic organic molecules on early Earth. In P. J. Thomas, R. D. Hicks, C. F. Chyba, & C. P. McKay (Eds.), *Comets and the origin and evolution of life* (2nd ed., pp. 169–206). Springer. https://doi.org/10.1007/10903490_6

Cook, G. E. (1965). Satellite drag coefficients. *Planetary and Space Science*, *13*(10), 929–946. https://doi.org/10.1016/0032-0633(65)90150-9

DeLuca, M., Munsat, T., Thomas, E., & Sternovsky, Z. (2018). The ionization efficiency of aluminum and iron at meteoric velocities. *Planetary and Space Science*, *156*, 111–116. https://doi.org/10.1016/j.pss.2017.11.003

DeLuca, M., & Sternovsky, Z. (2019). High-speed drag measurements of aluminum particles in free molecular flow. *Journal of Geophysical Research: Space Physics*, *124*(5), 3743–3751. https://doi.org/10.1029/2019JA026583

Elford, W. G., Steel, D. I., & Taylor, A. D. (1997). Implications for meteoroid chemistry from the height distribution of radar meteors. *Advances in Space Research*, *20*(8), 1501–1504. https://doi.org/10.1016/S0273-1177(97)00425-0

Fielding, L. A., Hillier, J. K., Burchell, M. J., & Armes, S. P. (2015). Space science applications for conducting polymer particles: Synthetic mimics for cosmic dust and micrometeorites. *Chemical Communications*, *51*(95), 16886–16899. https://doi.org/10.1039/C5CC07405C

Flynn, G. J., Keller, L. P., Jacobsen, C., & Wirick, S. (2004). An assessment of the amount and types of organic matter contributed to the Earth by interplanetary dust. *Advances in Space Research*, *33*(1), 57–66. https://doi.org/10.1016/j.asr.2003.09.036

Flynn, G. J., Wirick, S., & Keller, L. P. (2013). Organic grain coatings in primitive interplanetary dust particles: Implications for grain sticking in the Solar Nebula. *Earth Planets and Space*, *65*(10), 1159–1166. https://doi.org/10.5047/eps.2013.05.007

Glavin, D. P., & Bada, J. L. (2001). Survival of amino acids in micrometeorites during atmospheric entry. *Astrobiology*, *1*(3), 259–269. https://doi.org/10.1089/15311070152757456

Goldsworthy, B. J., Burchell, M. J., Cole, M. J., Armes, S. P., Khan, M. A., Lascelles, S. F., et al. (2003). Time of flight mass spectra of ions in plasmas produced by hypervelocity impacts of organic and mineralogical microparticles on a cosmic dust analyser. *Astronomy & Astrophysics*, *409*(3), 1151–1167. https://doi.org/10.1051/0004-6361:20031087

Gómez Martín, J. C., Bones, D. L., Carrillo-Sánchez, J. D., James, A. D., Trigo-Rodríguez, J. M., Fegley, B., Jr., & Plane, J. M. C. (2017). Novel experimental simulations of the atmospheric injection of meteoric metals. *The Astrophysical Journal*, *836*(2), 212. https://doi.org/10.3847/1538-4357/aa5c8f

Hawkes, R. L., & Jones, J. (1975). A quantitative model for the ablation of dustball meteors. *Monthly Notices of the Royal Astronomical Society*, *173*(2), 339–356. https://doi.org/10.1093/mnras/173.2.339

Hillier, J. K., Sternovsky, Z., Armes, S. P., Fielding, L. A., Postberg, F., Bugiel, S., et al. (2014). Impact ionisation mass spectrometry of polypyrrole-coated pyrrhotite microparticles. *Planetary and Space Science*, *97*, 9–22. https://doi.org/10.1016/j.pss.2014.04.008

Janches, D., Bruzzone, J. S., Pokorný, P., Carrillo-Sanchez, J. D., & Sarantos, M. (2020). A comparative modeling study of the seasonal, temporal, and spatial distribution of meteoroids in the upper atmospheres of Venus, Earth, and Mars. *The Planetary Science Journal*, *1*(3), 59. https://doi.org/10.3847/psj/abba35

Janches, D., Dyrud, L. P., Broadley, S. L., & Plane, J. M. C. (2009). First observation of micrometeoroid differential ablation in the atmosphere. *Geophysical Research Letters*, *36*(6), 145. https://doi.org/10.1029/2009gl037389

Janches, D., Plane, J. M. C., Nesvorný, D., Feng, W., Vokrouhlický, D., & Nicolls, M. J. (2014). Radar detectability studies of slow and small zodiacal dust cloud particles. I. The case of Arecibo 430 MHz meteor head echo observations. *The Astrophysical Journal*, *796*(1), 41. https://doi.org/10.1088/0004-637x/796/1/41

Janches, D., Swarnalingam, N., Carrillo-Sanchez, J. D., Gomez-Martin, J. C., Marshall, R., Nesvorný, D., et al. (2017). Radar detectability studies of slow and small zodiacal dust cloud particles. III. The role of sodium and the head echo size on the probability of detection. *The Astrophysical Journal*, *843*(1), 1. https://doi.org/10.3847/1538-4357/aa775c

Janches, D., Swarnalingam, N., Plane, J. M. C., Nesvorný, D., Feng, W., Vokrouhlický, D., & Nicolls, M. J. (2015). Radar detectability studies of slow and small zodiacal dust cloud particles. II. A study of three radars with different sensitivity. *The Astrophysical Journal*, *807*(1), 13. https://doi.org/10.1088/0004-637x/807/1/13

Jenniskens, P., Schaller, E. L., Laux, C. O., Wilson, M. A., Schmidt, G., & Rairden, R. L. (2004). Meteors do not break exogenous organic molecules into high yields of diatomics. *Astrobiology*, *4*(1), 67–79. https://doi.org/10.1089/153110704773600249

Jenniskens, P., Wilson, M. A., Packan, D., Laux, C. O., Krüger, C. H., Boyd, I. D., et al. (2000). Meteors: A delivery mechanism of organic matter to the early Earth. *Earth, Moon, and Planets*, *82–83*, 57–70. https://doi.org/10.1023/A:1017017728166

Koschny, D., Soja, R. H., Engrand, C., Flynn, G. J., Lasue, J., Levasseur-Regourd, A.-C., et al. (2019). Interplanetary dust, meteoroids, meteors and meteorites. *Space Science Reviews*, *215*(4), 34. https://doi.org/10.1007/s11214-019-0597-7

Li, Y. W., Bugiel, S., Trieloff, M., Hillier, J. K., Postberg, F., Price, M. C., et al. (2014). Morphology of craters generated by hypervelocity impacts of micron-sized polypyrrole-coated olivine particles. *Meteoritics & Planetary Sciences*, *49*(8), 1375–1387. https://doi.org/10.1111/maps.12338

Lias, S. G. (2021). Ionization energy evaluation. In P. J. Linstrom, & W. G. Mallard (Eds.), *NIST chemistry WebBook, NIST standard reference database number 69*. National Institute of Standards and Technology. (retrieved December 15, 2021). https://doi.org/10.18434/T4D303

Lifshitz, A., Tamburu, C., & Suslensky, A. (1989). Isomerization and decomposition of pyrrole at elevated temperatures: Studies with a single-pulse shock tube. *The Journal of Physical Chemistry*, *93*(15), 5802–5808. https://doi.org/10.1021/j100352a030

Luo, Y.-R., & Cheng, J.-P. (2019). Bond dissociation energies. In J. R. Rumble (Ed.), *CRC handbook of chemistry and physics* (100th ed.). CRC Press/Taylor & Francis.

Mathews, J. D., Meisel, D. D., Hunter, K. P., Getman, V. S., & Zhou, Q. (1997). Very high resolution studies of micrometeors using the Arecibo 430 MHz radar. *Icarus*, *126*(1), 157–169. https://doi.org/10.1006/icar.1996.5641

McNeil, W. J., Lai, S. T., & Murad, E. (1998). Differential ablation of cosmic dust and implications for the relative abundances of atmospheric metals. *Journal of Geophysical Research*, *103*(D9), 10899–10912. https://doi.org/10.1029/98JD00282

Murray, I. S., Hawkes, R. L., & Jenniskens, P. (1999). Airborne intensified charge-coupled device observations of the 1998 Leonid shower. *Meteoritics & Planetary Sciences*, *34*(6), 949–958. https://doi.org/10.1111/j.1945-5100.1999.tb01413.x

Nesvorný, D., Janches, D., Vokrouhlický, D., Pokorný, P., Bottke, W. F., & Jenniskens, P. (2011). Dynamical model for the zodiacal cloud and sporadic meteors. *The Astrophysical Journal*, *743*(2), 129. https://doi.org/10.1088/0004-637x/743/2/129

Nesvorný, D., Jenniskens, P., Levison, H. F., Bottke, W. F., Vokrouhlický, D., & Gounelle, M. (2010). Cometary origin of the zodiacal cloud and carbonaceous micrometeorites. Implications for hot debris disks. *The Astrophysical Journal*, *713*(2), 816–836. https://doi.org/10.1088/0004-637x/713/2/816

Picone, J. M., Hedin, A. E., Drob, D. P., & Aikin, A. C. (2002). NRLMSISE-00 empirical model of the atmosphere: Statistical comparisons and scientific issues. *Journal of Geophysical Research*, *107*(A12), 1468. https://doi.org/10.1029/2002JA009430

Plane, J. M. C. (2012). Cosmic dust in the Earth's atmosphere. *Chemical Society Reviews*, *41*(19), 6507–6518. https://doi.org/10.1039/c2cs35132c

Riebe, M. E. I., Foustoukos, D. I., Alexander, C. M. O. 'D., Steele, A., Cody, G. D., Mysen, B. O., & Nittler, L. R. (2020). The effects of atmospheric entry heating on organic matter in interplanetary dust particles and micrometeorites. *Earth and Planetary Science Letters*, *540*, 116266. https://doi.org/10.1016/j.epsl.2020.116266

Rietmeijer, F. J. M. (2002). Collected extraterrestrial materials: Interplanetary dust particles, micrometeorites, meteorites, and meteoric dust. In E. Murad, & I. P. Williams (Eds.), *Meteors in the Earth's atmosphere* (pp. 215–245). Cambridge University Press.

Shu, A., Collette, A., Drake, K., Grün, E., Horányi, M., Kempf, S., et al. (2012). 3 MV hypervelocity dust accelerator at the Colorado center for lunar dust and atmospheric studies. *Review of Scientific Instruments*, *83*(7), 075108. https://doi.org/10.1063/1.4732820

Spurný, P., Betlem, H., Jobse, K., Koten, P., & van't Leven, J. (2000). New type of radiation of bright Leonid meteors above 130 km. *Meteoritics & Planetary Sciences*, *35*(5), 1109–1115. https://doi.org/10.1111/j.1945-5100.2000.tb01497.x

Spurný, P., Betlem, H., Leven, J. V., & Jenniskens, P. (2000). Atmospheric behavior and extreme beginning heights of the thirteen brightest photographic Leonid meteors from the ground-based expedition to China. *Meteoritics & Planetary Sciences*, *35*(2), 243–249. https://doi.org/10.1111/j.1945-5100.2000.tb01773.x

Srama, R., Woiwode, W., Postberg, F., Armes, S. P., Fujii, S., Dupin, D., et al. (2009). Mass spectrometry of hyper-velocity impacts of organic micrograins. *Rapid Communications in Mass Spectrometry*, *23*(24), 3895–3906. https://doi.org/10.1002/rcm.4318

Sternovsky, Z. (2022). Differential ablation of organic coatings from micrometeoroids simulated in the laboratory. [Dataset]. Zenodo. https://doi.org/10.5281/zenodo.6369292

Swarnalingam, N., Janches, D., Carrillo-Sanchez, J. D., Pokorny, P., Plane, J. M. C., Sternovsky, Z., & Nesvorny, D. (2019). Modeling and altitude distribution of meteor head echoes observed with HPLA radars: Implications for the radar detectability of meteoroid populations. *The Astronomical Journal*, *157*(5), 179. https://doi.org/10.3847/1538-3881/ab0ec6

Thomas, E., Auer, S., Drake, K., Horányi, M., Munsat, T., & Shu, A. (2013). FPGA cross-correlation filters for real-time dust detection and selection. *Planetary and Space Science*, *89*, 71–76. https://doi.org/10.1016/j.pss.2013.09.004

Thomas, E., Horányi, M., Janches, D., Munsat, T., Simolka, J., & Sternovsky, Z. (2016). Measurements of the ionization coefficient of simulated iron micrometeoroids. *Geophysical Research Letters*, *43*(8), 3645–3652. https://doi.org/10.1002/2016GL068854

Thomas, E., Simolka, J., DeLuca, M., Horányi, M., Janches, D., Marshall, R. A., et al. (2017). Experimental setup for the laboratory investigation of micrometeoroid ablation using a dust accelerator. *Review of Scientific Instruments*, *88*(3), 034501. https://doi.org/10.1063/1.4977832

Vondrak, T., Plane, J. M. C., Broadley, S., & Janches, D. (2008). A chemical model of meteoric ablation. *Atmospheric Chemistry and Physics*, *8*(23), 7015–7031. https://doi.org/10.5194/acp-8-7015-2008